CCFE
CULHAM CENTRE FOR FUSION ENERGY

UK Atomic Energy Authority

UKAEA-CCFE-PR(21)05

W.W. Heidbrink, A. Garcia, W. Boeglin, M. Salewski

Phase-space Sensitivity (Weight Functions) of 3 MeV Proton Diagnostics

Phase-space Sensitivity (Weight Functions) of 3 MeV Proton Diagnostics

W.W. Heidbrink, A. Garcia, W. Boeglin, M. Salewski

This is a preprint of a paper submitted for publication in
Plasma Physics and Controlled Fusion

Phase-space Sensitivity (Weight Functions) of 3 MeV Proton Diagnostics

W.W. Heidbrink,[1] A. Garcia,[1], W. Boeglin,[2] M. Salewski,[3]

[1]University of California, Irvine, CA, USA

[2]Florida International University, FL, USA

[3]Department of Physics, Technical University of Denmark, Copenhagen, Denmark

ABSTRACT. The weight function $W(X)$ is a diagnostic sensitivity to phase-space variables X that relates the measured signal C to the distribution function $F(X)$ through the equation $C = \int W(X)F(X)\,dX$. In the present work, an algorithm to calculate W for a diagnostic that measures 3 MeV protons produced in d(d,p)t fusion reactions between a fast ion and a thermal deuteron is developed. The emitted protons escape the tokamak on curved orbits and are detected. These curved orbits constitute effective diagnostic "sightlines." The presented algorithm accounts for the complications associated with these curved sightlines. An initial calculation of time-reversed proton orbits computes effective solid angles and sightlines for the relevant range of incident proton velocity vectors. These precomputed orbits are then used within the framework of FIDASIM [Plasma Phys. Cont. Fusion **62** (2020) 105008] to calculate the reactivity averaged over the thermal distribution of the "target" deuterons and the probability that a fast ion of specified energy and pitch has a gyroangle that is consistent with the kinematic equations along each of the sightlines. Comparisons with analytic formulas and with independent calculations for the MAST 3-MeV proton diagnostic verify the algorithm.

1 Introduction

The weight function plays a key role in Energetic Particle research. The weight function $W(X)$ describes the sensitivity to phase-space variables X of a diagnostic signal and is used in forward modeling of expected signals [1], in tomographic inversions to infer the distribution function [2] and for qualitative interpretation of experimental dependencies [3]. Mathematically, W determines which portions of the energetic particle distribution function $F(X)$ contribute to a measured signal C,

$$C = \int W(X)F(X)\,dX. \tag{1}$$

Weight functions have already been developed for many fast-ion diagnostics such as fast-ion D-alpha (FIDA) [4, 5], collective Thomson scattering [6], neutral particle analyzer (NPA) [1, 7], neutron [8, 9, 10], gamma-ray [11, 12] and fast-ion loss detector [13] diagnostics. In the present work, an algorithm to calculate W for a 3 MeV proton diagnostic such as

the one at MAST [14] is developed. To date, the majority of these weight functions were developed for two-dimensional velocity space but recent work [5] utilizes three-dimensional orbit weight functions.

The MAST diagnostic measures 3 MeV protons produced in d(d,p)t fusion reactions between fast ions and thermal deuterons in the plasma core. The emitted protons escape the tokamak on curved orbits, pass through a collimating structure, and are detected. Conceptually, the calculation is analogous to calculation of the weight function of a neutron spectrometer but there are complications. Unlike with neutrons, photons, or neutrals, the "sightlines" are curved trajectories that depend upon the proton velocity; the orbit curvature also alters the solid angle accepted by the collimator. A further complication is that the energy of the emitted proton depends upon the velocities of the reactants and the direction of emission, so the "sightline" itself depends upon the reaction kinematics, with the consequence that different proton energies probe different phase-space volumes. Because the d-d reaction is anisotropic, the reaction probability also depends upon these velocities.

The presented algorithm takes all of these complications into account. Section 2 provides an overview of the approach. Section 3 explains how to compute the effective solid angle of the curved "sightlines" that are accepted by the collimating structure. Calculation of the rate of relevant d-d reactions involves two steps: the basic reaction rate (Sec. 4.1) and determination of the portion of the fast-ion population that produces a proton with the measured energy and trajectory (Sec. 4.2). The computational approach adopted to calculate these weight functions is described in Sec. 5, followed by verification of the calculations in Sec. 6. Section 7 contains formulas for velocity-space and orbit weight functions and shows an example for a MAST detector. Conclusions appear in Sec. 8.

2 Formulation of the problem

If the signal-to-noise ratio of the instrument permits, the measured quantity is an energy-resolved count rate at the detector. We express the d-d reaction in standard nuclear physics notation 2(1,3)4, where particle 2 is the thermal deuterium, particle 1 is the fast ion, particle 3 is the 3-MeV proton, and particle 4 is the triton. Our concern is the d(d,p)t reaction so $m_1 = m_2 = 2m_p$, $m_3 = m_p$ and $m_4 = 3m_p$, with m_p the proton mass. The measured energy-resolved count rate is $C(E_3, \Delta E_{bin})$, where E_3 is the proton energy and ΔE_{bin} is the energy resolution of the measurement.

A limitation of the present work is that the calculated weight function applies exclusively to reactions between an energetic "fast-ion" population and a slower, thermal population. In other words, the fast-ion (particle 1) is the beam, particle 2 is a thermal deuterium reactant, particle 3 is the measured 3-MeV proton, and particle 4 is undetected. This

type of reaction is customarily called "beam-plasma" in fusion research. In reality, "beam-beam" reactions between pairs of fast ions and "thermonuclear" reactions between pairs of thermal deuterons also occur; in both of these situations, the two reacting ions often have comparable speeds. Since the beam-plasma reaction rate depends linearly on the fast-ion distribution function, its weight function is well-suited for tomographic inversion to infer the distribution function using standard matrix methods; this is not true for beam-beam reactions. However, on two devices where 3-MeV proton diagnostics are currently implemented or planned, MAST-U [14] and NSTX-U [15], beam-plasma reactions predominate. For example, in the L-mode NSTX-U plasma of [16], beam-beam reactions constitute $< 11\%$ and thermonuclear reactions constitute $< 1\%$ of the total rate.

Since the escaping proton orbits are collisionless, the phase-space volume accepted by the detector can be related to the phase-space volume traversed by the curved "sightlines," so the measured count rate is [17]

$$C(E_3, \Delta E_{bin}) = \int\int\int dl\, dA\, d\Omega\, S(\mathbf{r}, \mathbf{v}_1, \mathbf{v}_2, \mathbf{v}_3), \tag{2}$$

where $\int dl$ represents integration over the sightline, $\int dA$ represents integration over the detector area, $\int d\Omega$ represents integration over the solid angle accepted by the collimating structure, and $S(\mathbf{r}, \mathbf{v}_1, \mathbf{v}_2, \mathbf{v}_3)$ represents the emissivity (in reactions/volume-time) of protons that are emitted at position $\mathbf{r}$ along the sightline with the correct values of E_3 and solid angle. As in the formulation of the weight function for a neutron collimator [8], the emissivity can be divided into two pieces, one piece that describes the d-d reactivity for the selected reaction kinematics, and another piece that describes the number of fast ions that can produce a proton with the velocity $\mathbf{v}_3$ accepted by the specified sightline,

$$S(\mathbf{v}_3, \mathbf{r}) = \int d\mathbf{v}_1 \int d\mathbf{v}_2\, R(\mathbf{v}_1, \mathbf{v}_2, \mathbf{v}_3, \mathbf{r}) p_{gyro}(\mathbf{v}_1, \mathbf{v}_2, \mathbf{v}_3) f_1(\mathbf{v}_1, \mathbf{r}) f_2(\mathbf{v}_2, \mathbf{r}). \tag{3}$$

The emissivity R depends upon the d-d cross section (including anisotropy), the relative velocities of the reactants $|\mathbf{v}_1 - \mathbf{v}_2|$, and the emitted proton's velocity $\mathbf{v}_3$. In Sec. 4.1, the integration over the distribution function f_2 of the target deuterons is incorporated into the emissivity R, making R a function of the ion temperature T_i, the rotation velocity $\mathbf{v}_{rot}$, and the deuterium target density n_d. In this work, the fast-ion distribution function f_1 is represented by a guiding-center distribution function $F(v_\parallel, v_\perp, \mathbf{r})$; the third velocity coordinate, the gyroangle γ associated with the fast gyromotion, is assumed of uniform probability and is not explicitly shown. (Here, $v_\parallel$ is the component of the fast-ion velocity along the magnetic field $\mathbf{B}$ and $v_\perp$ is the magnitude of the perpendicular velocity.)

The function $p_{gyro}(\mathbf{v}_1, \mathbf{v}_2, \mathbf{v}_3)$ represents the probability density that the gyroangle of the fast ion has the correct value to produce the measured proton. In practice, it is advantageous [8] to consider intervals of speed v_3 (or proton energy E_3). If v_3 is interpreted

this way, p_{gyro} represents the probability that the selected fast ion has a gyroangle that produces protons within the specified range of speeds.

Recall from Eq. 1 that the weight function is defined through the relation $C(E_3) = \int W(X, E_3)F(X)\,dX$. The goal of the following sections is to simplify and rearrange Eqs. 2 and 3 into the form of Eq. 1 in order to extract the weight function W. To that end, the next section explains how to simplify and calculate the $\int\int\int dl\,dA\,d\Omega$ term that describes the sightlines and collimating structure. The emissivity R is simplified in Sec. 4.1 and formulas for the probability p_{gyro} are given in Sec. 4.2.

3 "Sightlines" selected by the collimating structure

The treatment of the sightlines follows [17]. Figure 1 illustrates the bundles of "rays" collected by four MAST proton detectors in a particular equilibrium. Although the effective solid angle is largest for a central sightline, protons have a finite probability of striking the detector for a range of different incident velocity vectors. An orbit code calculates the trajectory represented by $\int dl$. Since the orbit is collisionless, time is reversed in the calculation in order to calculate orbits backward from the detector into the plasma. Each trajectory has an effective weight represented by the product $\int\int dA\,d\Omega$. Since the magnetic field changes little on the scale of the collimating structure, incident orbits with the same velocity can be considered identical over the entire area of the detector. With this approximation, we can replace $\int\int dA\,d\Omega$ by $\mathrm{A}\int T(\Omega)\,d\Omega$, where the transmission function $T(\Omega)$ is proportional to the fraction of the detector area "illuminated" by a particular incident velocity vector.

Define a central velocity vector on the axis of the collimator, i.e., from the center of the aperture to the center of the detector. Our goal is to compute $AT(\Omega)$ for a representative sample of orbits that strike the detector. Consider a cylindrical collimating structure of radius a and length d (Fig. 2a). If the orbits were straight, velocity vectors that tilt from the collimator axis by $\tan(2a/d)$ strike the edge of the detector. Select velocity vectors that travel from the center of the detector to points on the aperture plane. Since the actual orbits are curved, expand the area of the candidate points on the aperture plane by an amount $\delta a = \rho - \sqrt{\rho^2 - d^2}$, where ρ is the gyroradius, ensuring that all possible velocity vectors are considered. Use the sunflower algorithm that includes judiciously selected boundary points [18] to uniformly sample velocity vectors on this plane. For each velocity vector, calculate the actual orbit between the aperture plane and the center of the detector. Next, to determine the fraction of the detector area "illuminated" by this velocity, use the sunflower algorithm to uniformly sample positions on the detector plane. Shift the orbit to various positions on the detector plane to calculate the fraction of the detector area that is illuminated by this velocity vector. Figure 2b shows the portion of the detector area

illuminated by a particular incident velocity vector. This fraction is proportional to the desired transmission function $T(\Omega)$.

To check the accuracy of this calculation, replace the actual curved orbits with straight orbits. In this case, for small a/d, the program correctly calculates that $\int\int dA\, d\Omega = (\pi a^2)^2/d^2$, a familiar result in geometrical optics.

The output of this calculation is a set of velocity vectors at the detector that have non-zero transmission weights T. For each of these velocity vectors, follow the proton orbit backwards in the equilibrium field. For each channel, this bundle of curved trajectories constitutes the detector field of view or "sightline."

Note that the measured sightlines depend upon the proton energy. Typical changes in energy (Sec. 4) shift the trajectory through the plasma by a few centimeters radially (Fig. 3). Although the shift is modest, the fast-ion distribution function often has a large density gradient, so the shift in orbit must be properly treated. The transmission factors T also depend upon proton energy (Fig. 4), so this dependence is also taken into account.

4 Reaction kinematics and probability

For the reaction 2(1,3)4, particle 2 is the thermal deuterium, particle 1 is the fast ion, particle 3 is the 3-MeV proton, and particle 4 is the triton. The energy of the proton (Eq. 29 of [19]) is

$$E_3 = \frac{3}{4}(Q+K) + V\cos\theta\sqrt{\frac{3}{2}(Q+K)m_p} + \frac{1}{2}m_p V^2, \tag{4}$$

where $Q = 4.04$ MeV, $K = \frac{1}{2}m_p|\mathbf{v}_1 - \mathbf{v}_2|^2$, $\mathbf{V} = \frac{1}{2}(\mathbf{v}_1 + \mathbf{v}_2)$ is the center-of-mass velocity, and θ is the angle between $\mathbf{V}$ and the proton velocity in the center-of-mass frame $\mathbf{v}_3'$.

For a 100 keV deuterium beam (a relatively large value for positive neutral beam sources) interacting with typical values of $\mathbf{v}_2$, $K \lesssim 0.05$ MeV, a small value.

The first term on the right-hand side (RHS) of Eq. 4 gives the nominal proton energy of 3.03 MeV. The shift in energy from the nominal value is determined almost entirely by the middle term on the RHS. The largest absolute value of the middle term occurs for $\cos\theta = \pm 1$, so the shift in energy of the proton from the nominal 3.03 MeV value is

$$\Delta E_3 \simeq \frac{1}{2}v_1\sqrt{\frac{3}{2}Qm_p} = \frac{1}{2}\sqrt{\frac{3}{2}E_1 Q} \lesssim 0.39 \text{ MeV}, \tag{5}$$

for $E_1 = m_p v_1^2 = \frac{1}{2}m_D v_1^2 \simeq 0.10$ MeV. This implies that the fractional change in energy is $\Delta E_3/E_3 \lesssim 13\%$. Equation 5 determines the energies E_3 for which the proton spectrum is calculated.

At any particular location in the plasma, both the orientation and energy of the proton is known, so the proton velocity vector in the lab frame $\mathbf{v}_3$ is a known quantity in the following calculations.

4.1 Emissivity R

The goal of this subsection is to simplify the fusion emissivity $R(\mathbf{v}_1, \mathbf{v}_2, \mathbf{v}_3, \mathbf{r})$ that appears in Eq. 3.

There are three relevant rest frames. The proton velocity $\mathbf{v}_3$ is known in the lab frame. The effect of the target distribution function $f_2(\mathbf{v}_2)$ on the reaction rate is most easily computed in the rotating plasma frame. The effect of anisotropy is known in the center-of-mass frame.

The first step is to eliminate the integral over $\mathbf{v}_2$ that appears in Eqs. 2 and 3. To do so, replace $\int \sigma v(|\mathbf{v}_1 - \mathbf{v}_2|) f_2(\mathbf{v}_2, \mathbf{r})\, d\mathbf{v}_2$ by $n_d \langle \sigma v \rangle$, the emissivity after averaging over the target distribution. (Both n_d and the reactivity $\langle \sigma v \rangle$ are functions of position.) In the plasma frame, the velocity of the fast ion is $\mathbf{v}_1^{pl} = \mathbf{v}_1 - \mathbf{v}_{rot}$. To evaluate $\langle \sigma v \rangle$ we use Eqs. 8 and 9 of Bosch and Hale [20], using the coefficients given in their Table IV for the cross-section σ, with v_1^{pl} for the projectile speed, and average σv over a Maxwellian target that has temperature T_i. The resulting $\langle \sigma v \rangle$ is a function of $\mathbf{v}_1$, $\mathbf{v}_{rot}$, and T_i.

The d(d,p)t reaction is anisotropic. Brown and Jarmie [21] parameterize the differential cross section in the center-of-mass frame by

$$\sigma(\theta) = a + b \cos^2 \theta + c \cos^4 \theta. \tag{6}$$

The coefficients a, b, and c are functions of energy and are given in their Table I. We know θ from

$$\cos \theta = \frac{\mathbf{V} \cdot \mathbf{v}_3'}{V v_3'}, \tag{7}$$

where the center-of-mass velocity $\mathbf{V}$ is

$$\mathbf{V} = \frac{1}{2}(\mathbf{v}_1 + \langle \mathbf{v}_2 \rangle) \simeq \frac{1}{2}(\mathbf{v}_1 + \mathbf{v}_{rot}) \tag{8}$$

and $\mathbf{v}_3' = \mathbf{v}_3 - \mathbf{V}$ is the proton velocity in the center-of-mass frame.

The relative velocity in the center-of-mass frame is $\mathbf{v}_1 - \mathbf{V}$. To get the Brown-Jarmie coefficients for this particular reaction use the relative energy to interpolate for a, b, and c. Our goal is to compute the effect of anisotropy on the Bosch-Hale value of $\langle \sigma v \rangle$ we have already found. If the reaction was isotropic, the integral of the differential cross section

over θ gives a total cross section that is proportional to $a + b/3 + c/5$, so the anisotropy enhancement/deficit factor is

$$\kappa = \frac{a + b\cos^2\theta + c\cos^4\theta}{a + b/3 + c/5}. \tag{9}$$

Therefore, the reactivity for this reaction is $\kappa\langle\sigma v\rangle$ and the emissivity is $n_d\kappa\langle\sigma v\rangle$.

4.2 Calculating p_{gyro}

The goal of this subsection is to determine the number of fast ions in velocity space that can produce a reaction with the specified value of $\mathbf{v}_3$.

Jacobsen *et al.* [8] calculated velocity-space weight functions for neutron spectroscopy using the d(d,n)^{3}He reaction. Since $\mathbf{v}_3$ is known, they found that the calculation is simpler in the lab frame than in the center-of-mass frame. For simplicity, they assumed negligible target velocity ($\mathbf{v}_2 = 0$) in their treatment of the reaction kinematics (but *not* in the calculation of R discussed in the previous subsection). In the following, we do not make this assumption but ultimately conclude that it is justified for typical parameters.

Following Jacobsen *et al.*, the weight function for a particular fast ion with velocity $(v_\perp, v_\parallel)$ [or (energy,pitch)] is proportional to a factor proportional to the reaction rate and a kinematics-dependent velocity-space factor. Symbolically, the velocity-space weight function $w(E_{p1}, E_{p2}, \phi, v_\parallel, v_\perp, \mathbf{v}_{rot}, \mathbf{r})$ is found for emitted proton energies between E_{p1} and E_{p2} that are emitted at an angle ϕ with respect to the magnetic field by a reaction between a fast ion with parallel and perpendicular velocities $v_\parallel$ and $v_\perp$ and target ions that rotate at $\mathbf{v}_{rot}$ and have temperature T_i at the spatial location $\mathbf{r}$. This weight function is the product of a reaction rate and a conditional probability that depends upon the reaction kinematics,

$$R(\phi, v_\parallel, v_\perp, \mathbf{v}_{rot}, T_i) \times \text{prob}(E_{p1} < E_3 < E_{p2} | \phi, v_\parallel, v_\perp, \mathbf{v}_{rot}). \tag{10}$$

For the conditional probability, two components of the fast-ion velocity $\mathbf{v}_1$ are known but the third component, the gyroangle γ, is not. The goal of the kinematics calculation is twofold: (1) Find which gyroangles can produce a proton with the specified value of $\mathbf{v}_3$ and (2) determine the value of $\cos\theta$ to use in Eq. 9. Since gyromotion is assumed uniform, the fraction of fast ions p_{gyro} with the specified values of $(v_\perp, v_\parallel)$ that can produce this proton is equal to

$$p_{gyro} = \frac{\Delta\gamma}{2\pi}, \tag{11}$$

where $\Delta\gamma$ represents the range of gyroangles that produces protons in a specified energy range, $E_{p,1} < E_3 < E_{p,2}$.

Including the plasma rotation but assuming zero temperature of the target species, the equations of energy and momentum conservation in the lab frame are

$$\frac{1}{2}m_1 v_1^2 + \frac{1}{2}m_2 v_{rot}^2 + Q = \frac{1}{2}m_4 v_4^2 + \frac{1}{2}m_3 v_3^2 \tag{12}$$

and

$$m_1 \mathbf{v}_1 + m_2 \mathbf{v}_{rot} = m_3 \mathbf{v}_3 + m_4 \mathbf{v}_4. \tag{13}$$

Use momentum conservation to eliminate v_4 in Eq. 12 and replace the masses with their values for the d(d,p)t reaction. Introduce coordinates $(\hat{a}, \hat{b}, \hat{c})$ where $\hat{b}$ is along the magnetic field, $\hat{a}$ is oriented along the perpendicular component of the emitted proton, and $\hat{c}$ is orthogonal to the other unit vectors. Choose the origin of the fast-ion gyroangle γ so $\cos\gamma = 1$ when the gyroangle is aligned with $\hat{a}$. The fast-ion velocity is

$$\mathbf{v}_1 = \hat{b}v_{\|} + \hat{a}v_{\perp}\cos\gamma + \hat{c}v_{\perp}\sin\gamma, \tag{14}$$

the proton velocity is

$$\mathbf{v}_3 = \hat{b}v_3\cos\phi + \hat{a}v_3\sin\phi \tag{15}$$

and the rotation velocity is

$$\mathbf{v}_{rot} = \hat{b}v_b + \hat{a}v_a + \hat{c}v_c. \tag{16}$$

After substitution, the equation for the gyroangle is

$$v_{\perp}(\sin\phi - \frac{2v_a}{v_3})\cos\gamma = v_3 - \frac{3Q}{2v_3 m_p} - (v_{\|}+v_b)\cos\phi - v_a\sin\phi - \frac{1}{2}\frac{v_1^2 + v_{rot}^2}{v_3} + \frac{2v_b v_{\|}}{v_3} - \frac{v_{rot}^2}{2v_3} + \frac{2v_c v_{\perp}\sin\gamma}{v_3}. \tag{17}$$

Since the last term on the right-hand side (RHS) is quite small, this equation is easy to solve iteratively for $\cos\gamma$.

For the anisotropy calculation, $\cos\theta$ is given by Eq. 7. All of the needed velocities are known.

In practice, the rotation velocity can be neglected in the calculation of γ and $\cos\theta$. Since Eq. 17 is solved for $\cos\gamma$, both a positive gyroangle γ_+ and a negative gyroangle γ_- satisfy the equation. If rotation is neglected, these angles are equal and opposite. With rotation, the final term in Eq. 17 that is proportional to $\sin\gamma$ causes an asymmetry between positive and negative gyroangles. However, as shown in Fig. 5a, even for a relatively large rotation velocity of 2×10^5 m/s, the difference in these angles is very small. Similarly (not shown), the center-of-mass angle $\cos\theta$ depends very weakly on the sign of γ.

To get p_{gyro}, we want to calculate a pair of gyroangles γ for two energies $E_{p,1}$ and $E_{p,2}$; this gives us an effective width in velocity space. (We actually want to calculate this pair for both γ_+ and γ_- but, since $\gamma_+ \simeq \gamma_-$, we can restrict the calculation to γ_+ and double its

probability.) Note that we do *not* want to calculate γ for two actual orbits with different E_3. Instead, we are interested in the *velocity-space* spread of fast-ion gyroangles that produce protons in a specified energy bin ΔE_{bin}. Use Eq. 17 to find γ_{high} for $E_{p,1} = E_3 + \Delta E_{bin}/2$ and γ_{low} for $E_{p,2} = E_3 - \Delta E_{bin}/2$. The gyroradius probability factor is

$$p_{gyro} \simeq \frac{|\gamma_{high} - \gamma_{low}|}{\pi}. \tag{18}$$

There are two potential pitfalls in the numerical calculation of γ from Eq. 17. One pitfall occurs when the factor $v_\perp(\sin\phi - 2v_a/v_3)$ on the LHS of Eq. 17 is zero. This occurs when the proton is emitted nearly parallel to the magnetic field or when $\mathbf{v}_1$ and $\mathbf{v}_3$ are nearly parallel or anti-parallel to each other; since both of these conditions occupy small velocity-space volumes, we set $p_{gyro} = 0$ for these special cases.

The second pitfall occurs when an energy bin extends beyond the maximum or minimum values of E_3 that are compatible with the other selected parameters. The maximum and minimum energies occur when the gyroangle is $\gamma = 0$ or $\gamma = \pi$. In these cases, Eq. 18 is replaced by $p_{gyro} = \gamma_{bin}$ when $\gamma \simeq 0$ or $p_{gyro} = \pi - \gamma_{bin}$ when $\gamma \simeq \pi$. Here, γ_{bin} is the value of γ evaluated at whichever edge of the energy bin has a value of proton energy permitted by the kinematics.

The maximum and minimum values of E_3 occur when $\cos\gamma \simeq \pm 1$ in Eq. 17. Use the quadratic formula to find that the minima and maxima values of the proton speed v_3 are

$$v_3 = \frac{-B + \sqrt{B^2 + 4C}}{2} \tag{19}$$

where

$$B = \mp v_\perp \sin\phi - (v_\parallel + v_b)\cos\phi - v_a \sin\phi$$

and

$$C = \frac{3}{2}\frac{Q}{m_p} + \frac{v_1^2 + v_{rot}^2}{2} - 2v_\parallel v_b \mp v_\perp v_a.$$

5 Implementation into the FIDASIM framework

Calculation of the 3 MeV proton count rate has been implemented within the framework of the FIDASIM synthetic diagnostic code [1]. Since detailed documentation is available on the FIDASIM GitHub website [22], only a brief summary is provided here.

Data preparation of input files in HDF5 format occurs outside of the framework of the FORTRAN FIDASIM code. As usual, plasma profiles, the fast-ion distribution function, and the equilibrium are prepared using Python or IDL data-preparation routines. The

FIDASIM Proton Table Inputs					
Member	Type	Rank	Dimension	Units	Description
nchan	Int	0	Scalar	unity	Number of detector channels
nrays	Int	0	Scalar	unity	Number of "rays"
nsteps	Int	0	Scalar	unity	Maximum number of orbit steps
nenergy	Int	0	Scalar	unity	Number of proton energies
earray	Float	1	[nenergy]	keV	Proton energies
daomega	Float	3	[nenergy,nrays,nchan]	cm^{-2}	Transmission factor
nactual	Float	3	[nenergy,nrays,nchan]	unity	Number of orbital spatial steps
sightline	Float	4	[nenergy,6,nsteps,nrays,nchan]	cm/s cm	Velocity and position in [r,phi,z]

Table 1: New inputs used by FIDASIM in the 3-MeV proton calculation.

additional input quantities for the 3-MeV proton calculation are the proton sightlines and transmission factors described in Sec. 3; they are listed in Table 1. The user specifies an array of energies for the proton spectrum. For each detector channel, "nrays" is the number of orbits to consider in the "bundle" of trajectories that strikes the detector. After reading the detector geometry and the equilibrium fields, a Lorentz orbit code calculates the time-reversed orbit (the "sightline") and an IDL code calculates the transmission factor ("daomega") for each specified "ray" for each detector. A typical calculation uses 150 orbital steps, 75 rays, and 11 proton energies.

Figure 6 shows a flowchart of the calculation within FIDASIM. After reading the input data, a routine converts the proton orbits (the "sightlines") into the Cartesian coordinate system utilized in FIDASIM. Next, bilinear interpolation is performed to find the fields and plasma parameters at each sightline step. Calculation of the probability factor and gyroangle described in Section 4.2 is the first major process in the algorithm. Inputs to subroutine `get_pgyro` are the magnetic field, proton energy, fast-ion energy, fast-ion pitch, plasma rotation and proton velocity. Although the plasma rotation is relatively small in Equation 17, it is kept in the computations for completeness.

Next, a gyro step is required to get the fast-ion density at the guiding center position. Since the fields, pitch and gyroangle are known, subroutine `pitch_to_vec` calculates the velocity of the fast ion. The velocity, beam mass and fields are then used to determine the

guiding center position in subroutine `gyro_step` using the formula for the gyroradius in [23]. Finally, the beam energy and pitch are used to calculate the guiding center fast-ion density at the gyro-step position.

Calculating the reaction rate is the last major process of the algorithm and follows the procedure outlined in Sec. 4.1. Linear interpolation is performed to determine the Brown-Jarmie coefficients for the given beam energy. FIDASIM reads in pre-calculated tables for the neutron and proton branches of the D-D beam-target fusion reaction. Bilinear interpolation is performed to calculate the proton production rate for a given thermal ion temperature and relative velocity between the fast ion and rotation velocities. Finally, the rate is multiplied by the thermal deuterium density.

After looping over detector channels, proton energies, orbit rays, and orbit steps, the code outputs proton spectra for each detector channel.

6 Code verification

This section discusses the selection of numerical parameters, the sensitivity of the output to two physics effects, and tests that verify that the code works properly. Two different sets of inputs that are representative of the MAST diagnostic installation are used for these tests. The first set is an artificial case that Netepenko used for the tests described in his Ph.D. thesis [15]. The second is for an actual MAST discharge, #29908. In both cases, the equilibrium is provided by EFIT [24] and the plasma parameters and distribution function are from TRANSP [25].

An initial test found that 5 proton energies is insufficient to resolve the proton spectrum but 13 energies provides adequate resolution. Increasing the number of orbital steps and number of rays did not significantly affect the results and slowed down the algorithm. Thus, nsteps=110 and nrays=50 are used in the following section.

In order to quantify the importance of the anisotropy correction factor, FIDASIM is run using anisotropic (Eq. 9) and isotropic ($\kappa = 1$) cross sections. Figure 7 shows that inclusion of the anisotropy of the d-d cross section makes a small difference of 4% for an injection energy of 50 keV for MAST conditions. Because many protons are emitted near the center-of-mass angle $\theta \simeq \pi/2$, where anisotropy reduces the cross section, the isotropic calculation is slightly higher. Since the effect of anisotropy grows with increasing energy, proper treatment of cross-section anisotropy is more important in facilities with higher injection energies or RF accelerated fast-ion tails.

Figure 8 compares the spectrum computed using the actual proton orbits to a calculation that utilizes the same orbits and transmission factors for all proton energies. Because higher-energy protons have larger gyroradii, they originate deeper in the plasma, where

the fast-ion and thermal densities are larger and the emissivity is larger. Conversely, lower-energy protons originate closer to the plasma edge where the emissivity is smaller. The result is that proper treatment of the orbits shifts the spectrum to higher energies (Fig. 8). The overall effect is modest for the MAST installation, however.

To benchmark the code, the calculated count rate was compared with an independent calculation using the formalism described in [15] for the inputs of MAST discharge #29908. The calculations differ by 2-5% for different channels.

As a second verification exercise, the proton spectrum was calculated for a monoenergetic, isotropic distribution function with cold thermal deuterons. This is a condition for which an analytical prediction of the expected spectrum is available [26]. The calculated spectrum has the predicted shape (Fig. 9).

7 Weight functions

The algorithm and program described so far computes the proton spectrum,

$$C(E_{p,1} < E_3 < E_{p,2}) \simeq A \int \int dl\, d\Omega\, T(\Omega) R p_{gyro} F(v_\parallel, v_\perp)\, dv_\parallel\, dv_\perp. \tag{20}$$

If we choose to evaluate the protons that come from a single position along the proton "sightline," (i.e., eliminate the integral over the sightline $\int dl$), Eq. 20 can be written as a set of factors that multiply the guiding-center fast-ion distribution function F. These factors constitute the velocity-space weight function w_{2D},

$$w_{2D}(E_3, v_\parallel, v_\perp, \mathbf{r}) = A \int d\Omega T(\Omega) R p_{gyro}. \tag{21}$$

Note that, although F is written as a function of $v_\parallel$ and $v_\perp$, it is straightforward to reexpress the velocities in terms of fast-ion energy E_1 and pitch $(v_\parallel/v)$ if one prefers. In addition to its dependence upon fast-ion velocity, w_{2D} depends upon spatial position along the line of sight.

For forward modeling with a specified guiding-center distribution function $F(v_\parallel, v_\perp, \mathbf{r})$, the expected signal is

$$C(E_{p,1} < E_3 < E_{p,2}) = \int dl \int \int dv_\parallel\, dv_\perp w_{2D} F. \tag{22}$$

The derived expression can also be used to find three-dimensional weight functions for orbit tomography [5] by appropriately weighting w_{2D} spatially based on the properties of the selected fast-ion orbits.

As an example, Fig. 10 shows velocity-space weight functions for a MAST detector. In this example, contributions to w_{2D} have been summed over the orbit to eliminate the spatial dependence of the weight function. The selected channel is the one with the largest toroidal velocity component in Fig. 1. Owing to the Doppler shift associated with the $\cos\theta$ term in Eq. 4, fast ions that move away from the detector emit protons of reduced energy, while fast ions that head toward the detector emit protons of increased energy. This is the reason that deuterons that travel in the direction of the toroidal field are more likely to produce a low-energy proton than deuterons that circulate against $\mathbf{B}$ in Fig. 10a. Conversely, high-energy protons are produced most effectively by deuterons that travel opposite to the toroidal field (Fig. 10c). Near the unshifted energy of 3.03 MeV, owing to the gyromotion, two peaks appear in the weight function (Fig. 10b). This occurs because one phase of the gyromotion can cancel the parallel component of motion along $\mathbf{B}$, while another phase cancels the opposite parallel motion. The shapes of these three proton-energy-resolved weight functions are qualitatively similar to the FIDA weight functions of [4] and are caused by geometrical effects associated with the gyromotion. If one integrates over energy, the pitch dependence of the weight function essentially disappears (Fig. 10d). However, owing to the strong energy dependence of the d-d fusion cross section, all proton energies exhibit a strong dependence on deuteron energy. (When integrated over proton energy and fast-ion pitch, the energy dependence of the weight function is close to the energy dependence of the d-d reactivity σv.) The proton signal is produced primarily by the highest energy ions in the deuterium distribution function.

Although resolving the 3-MeV proton energy spectrum is a technical challenge, Fig. 10 demonstrates that energy-resolved measurements provide valuable information about the deuterium distribution function.

8 Conclusion

An algorithm and computer program that calculates the count rate and weight function of a 3-MeV proton diagnostic has been developed and tested. The algorithm properly treats effects associated with curved proton orbits, as well as the anisotropy of the d-d cross section. The algorithm and program assumes that the proton signal is produced by beam-plasma reactions, rendering it inapplicable to plasmas with significant beam-beam or thermonuclear reaction rates.

In future work, the 3-MeV proton weight function will be employed in tomographic reconstructions of the fast-ion distribution function in MAST-U plasmas with proton, FIDA, neutron collimator, and neutral particle data.

Acknowledgements

We thank A. Netepenko for providing data for this study and L. Stagner for helpful suggestions. This work was supported by DOE grants DE-SC0019253 and DE-SC0001157 and NSF #1633631.

References

[1] GEIGER, B. et al., Plasma Phys. Controlled Fusion **62** (2020) 105008.

[2] SALEWSKI, M., NOCENTE, M., JACOBSEN, A. S., et al., Fusion Science Technology **74** (2018) 23.

[3] HEIDBRINK, W. W., LUO, Y., BURRELL, K. H., et al., Plasma Phys. Controlled Fusion **49** (2007) 1457.

[4] SALEWSKI, M., GEIGER, B., MOSEEV, D., et al., Plasma Phys. Controlled Fusion **56** (2014) 105005.

[5] STAGNER, L. and HEIDBRINK, W. W., Phys. Pl. **24** (2017) 092505.

[6] SALEWSKI, M., NIELSEN, S. K., BINDSLEV, H., et al., Nucl. Fusion **51** (2011) 083014.

[7] DU, X. D., VAN ZEELAND, M. A., HEIDBRINK, W. W., et al., Nucl. Fusion **60** (2020) 112001.

[8] JACOBSEN, A. S., SALEWSKI, M., ERIKSSON, J., et al., Nucl. Fusion **55** (2015) 053013.

[9] JACOBSEN, A. S., BINDA, F., CAZZANIGA, C., et al., Rev. Sci. Instrum. **88** (2017) 073506.

[10] SPERDUTI, A., CECCONELLO, M., et al., J. Instrumentation **14** (2019) C09005.

[11] SALEWSKI, M., NOCENTE, M., GORINI, G., et al., Nucl. Fusion **55** (2015) 093029.

[12] SALEWSKI, M., NOCENTE, M., GORINI, G., et al., Nucl. Fusion **56** (2016) 046009.

[13] GALDON-QUIROGA, J., GARCÍA-MUÕZ, M., SALEWSKI, M., et al., Plasma Phys. Controlled Fusion **60** (2018) 105005.

[14] PEREZ, R. V., BOEGLIN, W. U., DARROW, D. S., et al., Rev. Sci. Instrum. **85** (2014) 11D701.

[15] NETEPENKO, A., BOEGLIN, W. U., DARROW, D. S., ELLIS, R., and SIBILIA, M. J., Rev. Sci. Instrum. **87** (2016) 11D805.

[16] LIU, D., HEIDBRINK, W. W., et al., Nucl. Fusion **58** (2018) 082028.

[17] HEIDBRINK, W. W. and STRACHAN, J. D., Rev. Sci. Instrum. **56** (1985) 501.

[18] VOGEL, H., Mathematical Biosciences **44** (1979) 179.

[19] BRYSK, H., Plasma Physics **15** (1973) 611.

[20] BOSCH, H.-S. and HALE, G. M., Nucl. Fusion **32** (1992) 611.

[21] BROWN, R. E. and JARMIE, N., Physical Review C **41** (1990) 1391.

[22] https://d3denergetic.github.io/FIDASIM/.

[23] BELOVA, E. V., GORELENKOV, N. N., and CHENG, C. Z., Phys. Pl. **10** (2003) 3240.

[24] LAO, L. L., ST. JOHN, H., STAMBAUGH, R. D., KELLMAN, A. G., and PFEIFFER, W., Nucl. Fusion **25** (1985) 1611.

[25] http://w3.pppl.gov/transp/.

[26] HEIDBRINK, W. W., Nucl. Instrum. Methods Phys. Res. **A236** (1985) 380.

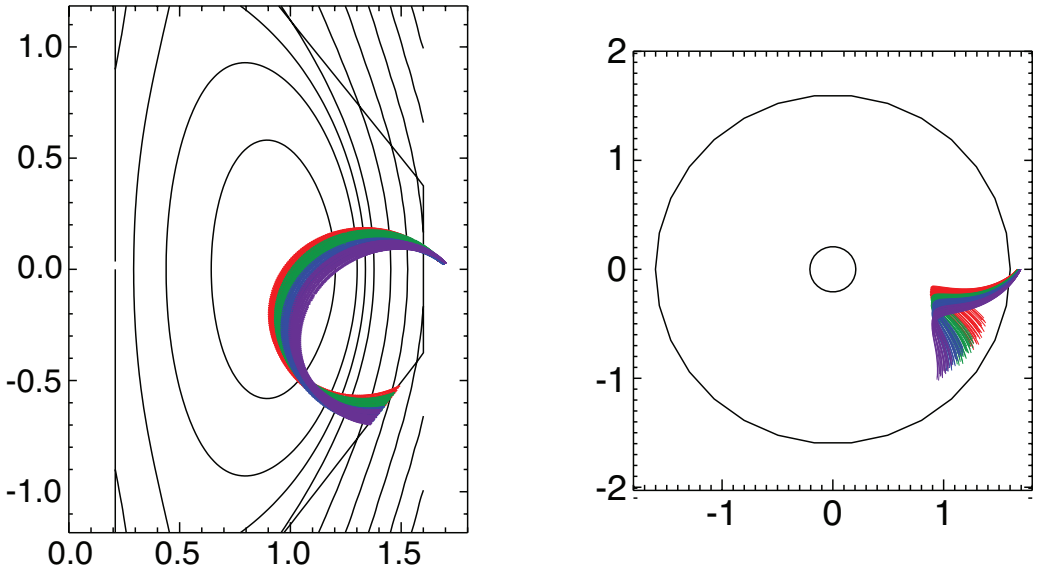

Figure 1: Elevation (left) and plan (right) views of 3.03 MeV proton orbits (colors) that reach the four MAST proton detectors in a particular equilibrium. The thickness of the lines is proportional to the effective transmission T. The black lines in the elevation represent flux surfaces.

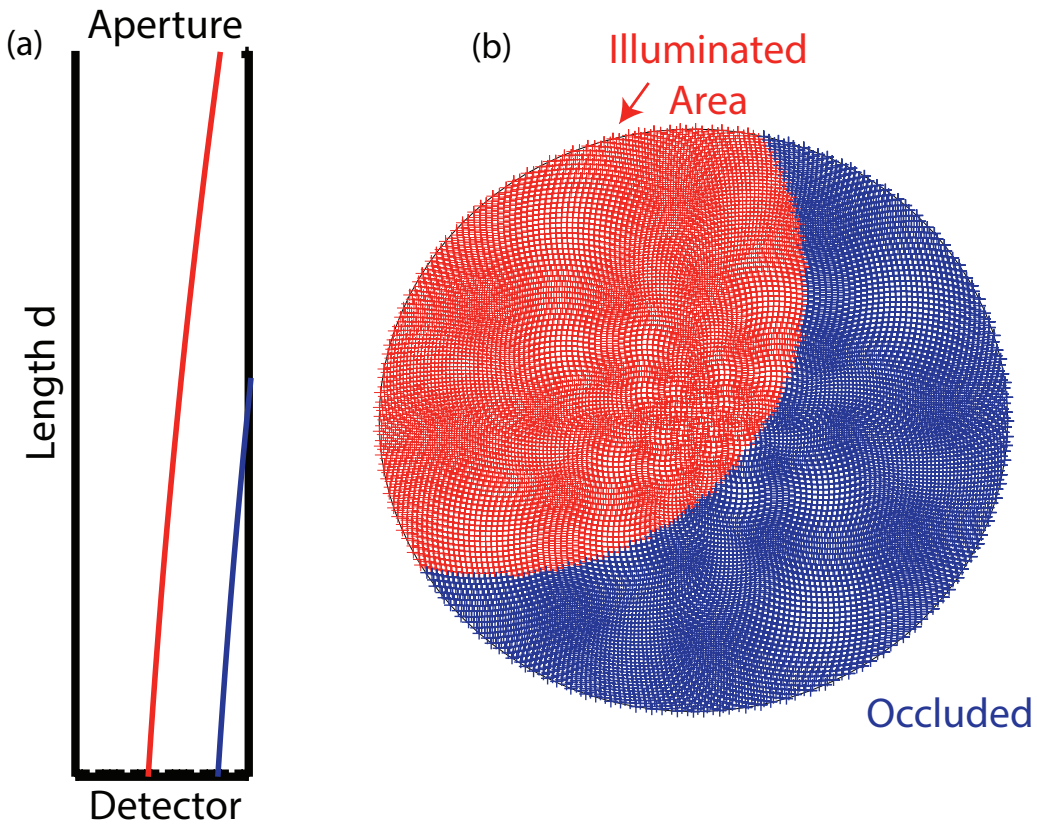

Figure 2: (a) Schematic diagram of a cylindrical collimator. For a given orientation of the incident proton velocity, some orbits reach the detector (red), while others do not (blue). (b) For a given incident velocity vector, only the red portion of the detector is illuminated. The figure also shows the sunflower sampling of the detector area.

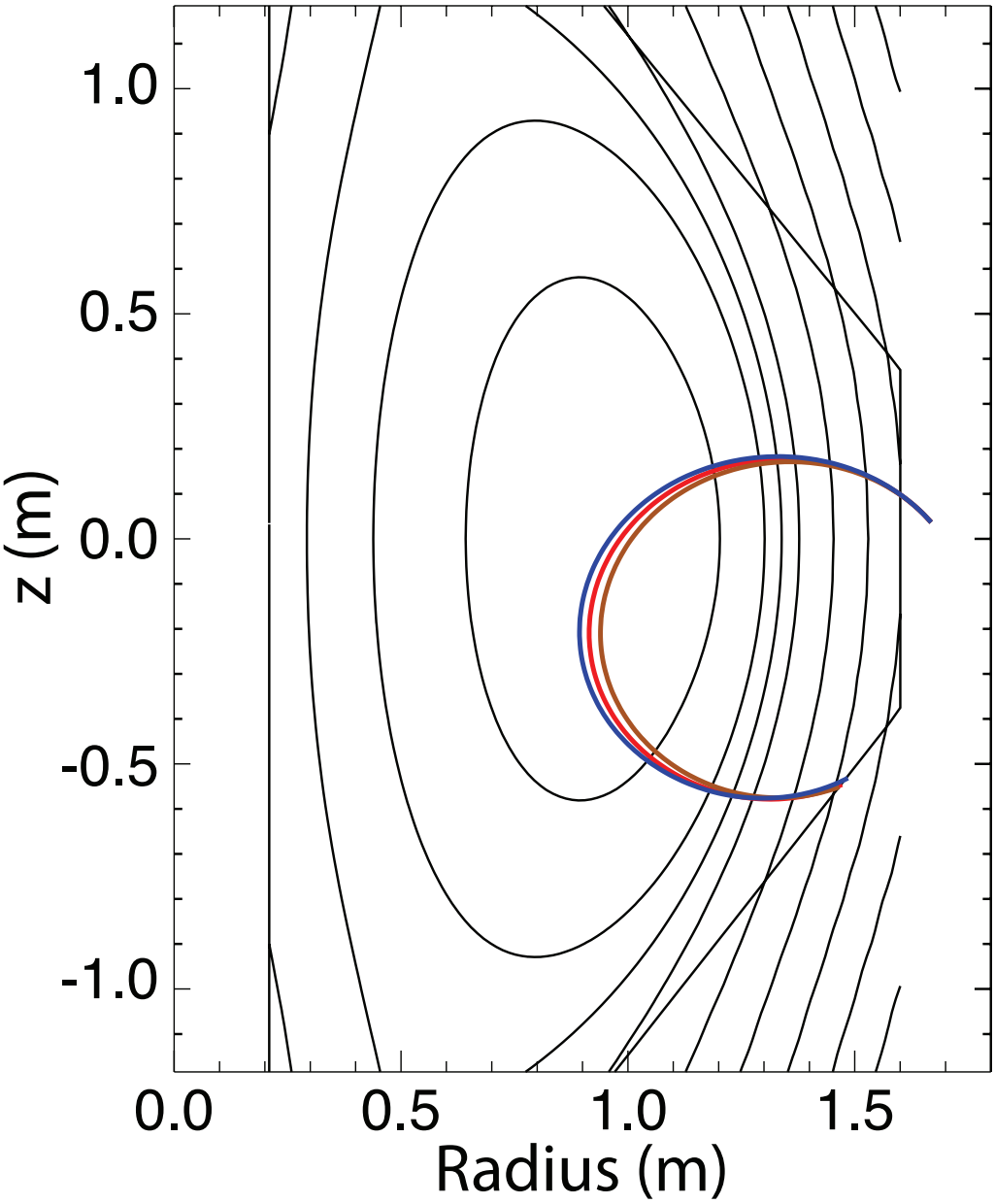

Figure 3: (R, z) projection of orbits that enter the detector with the same orientation for energies of 2730 (brown), 3030 (red), and 3330 keV (blue). The orbit shifts a few centimeters.

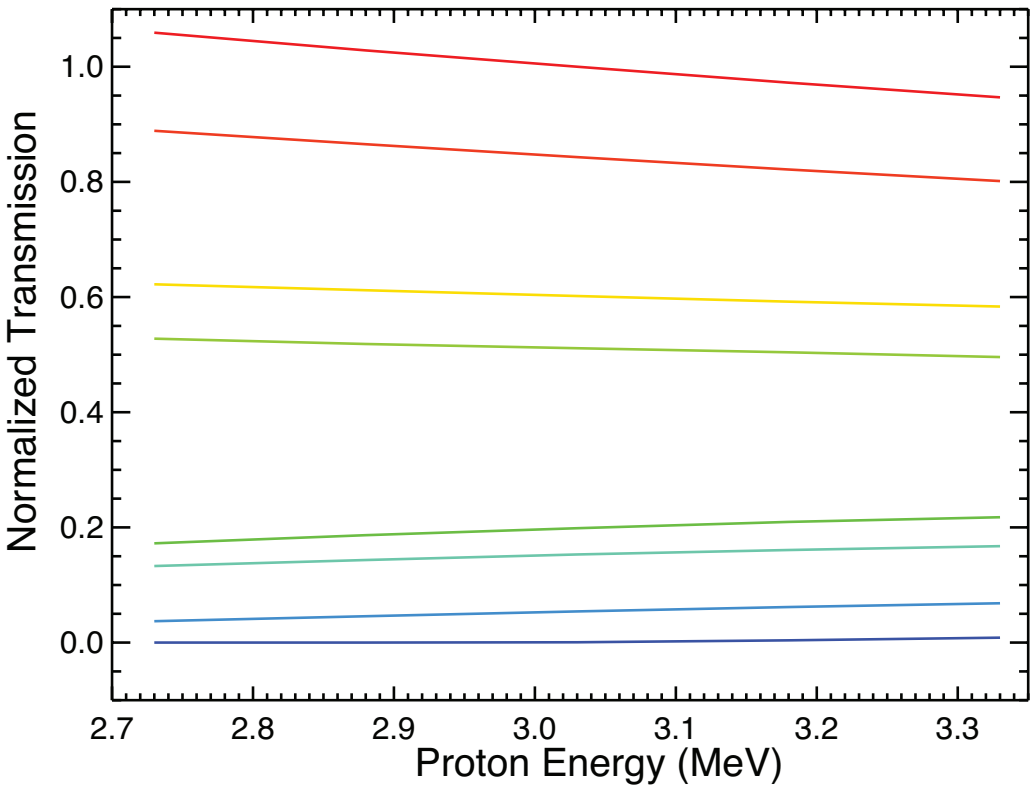

Figure 4: The overall transmission of the collimator increases with energy because the incident orbits are straighter. A variety of different incident velocity vectors are shown. The curves are normalized to the transmission of the maximum velocity vector for $E_3 =$ 3.03 MeV.

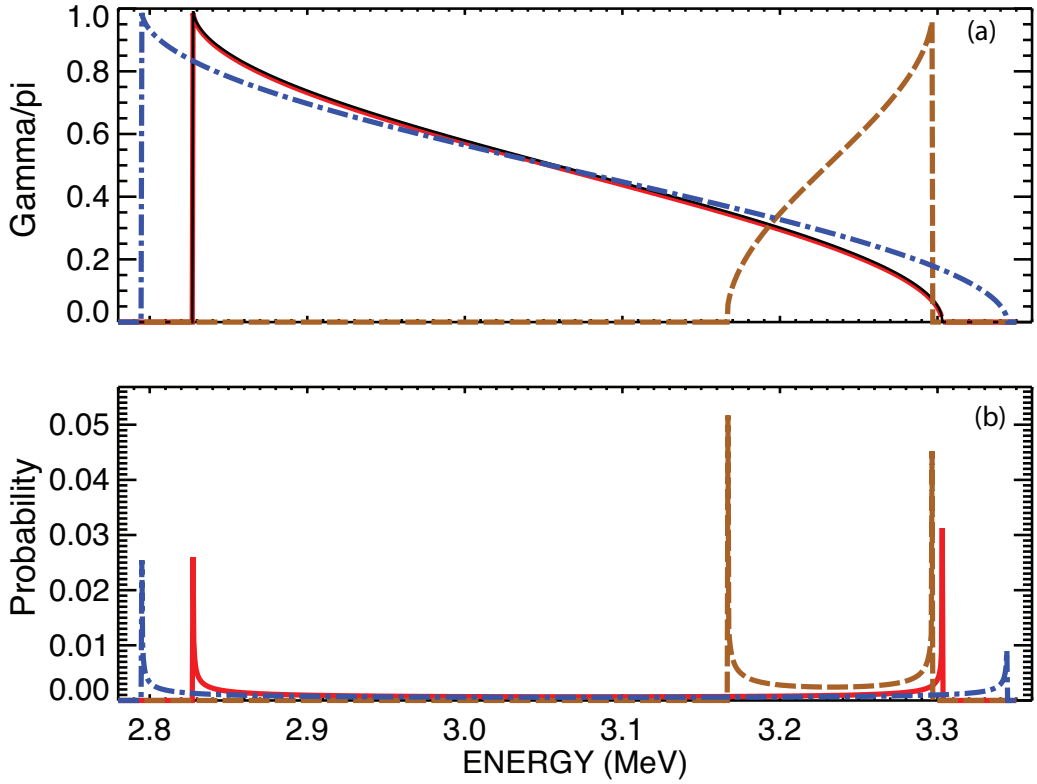

Figure 5: Dependence of (a) the absolute value of the normalized gyroradius $|\gamma|/\pi$ and (b) the probability of gyroradii in a specified energy range p_{gyro} on proton energy for $E_1 = 50$ keV and a rotation velocity of 2×10^5 m/s. Solid curves: lab-frame angle $\phi = \pi/2$ and fast ion pitch $v_\parallel/v = 0.5$. Dashed curves: $\phi = -\pi/4$ and $v_\parallel/v = 0.95$. Dot-dashed curves: $\phi = \pi/2$ and $v_\parallel/v = 0$. In (a), for the solid-line case, both γ_+ (red) and γ_- (black) are shown; the curves nearly overlay one another.

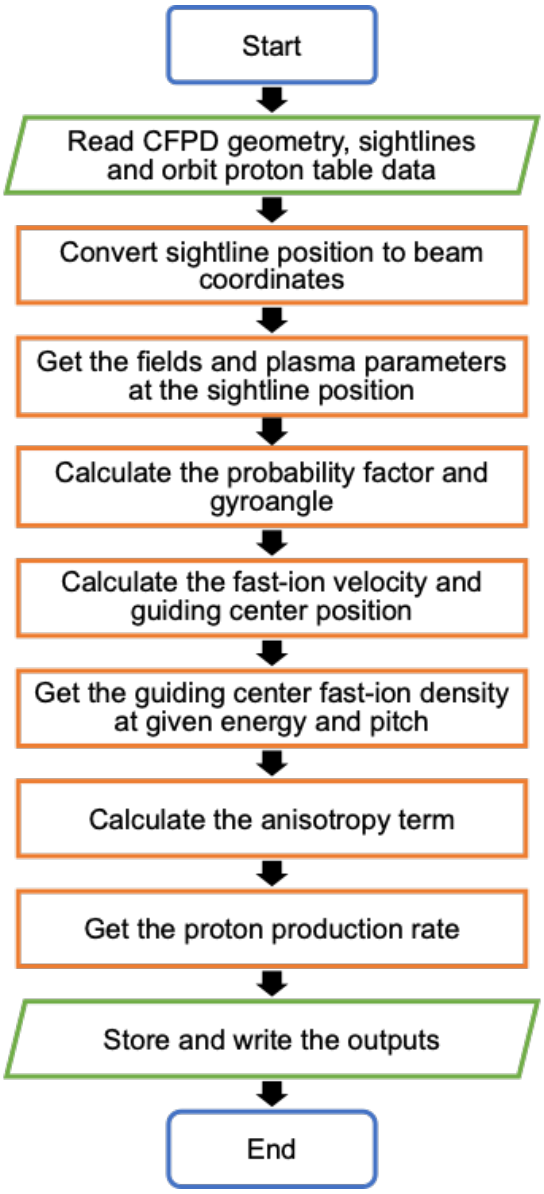

Figure 6: Flowchart for the portion of the algorithm that is implemented in the FORTRAN FIDASIM code.

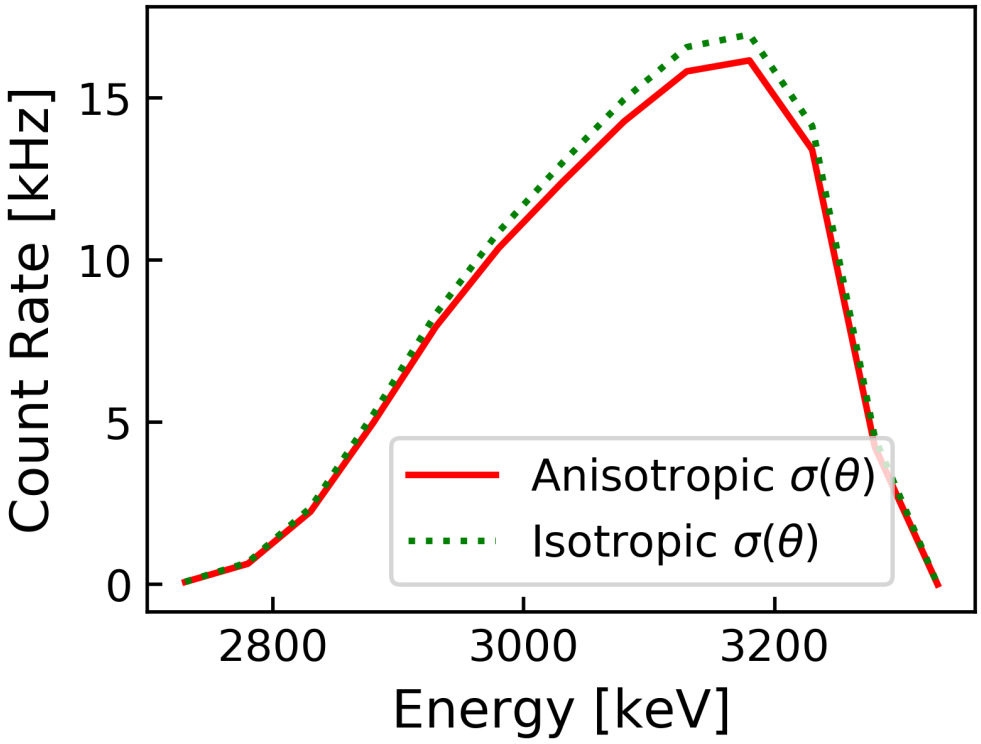

Figure 7: Comparison of the proton energy spectrum calculated using the actual anisotropic d-d cross section (solid curve) with a calculation that ignores cross-section anisotropy (dashed).

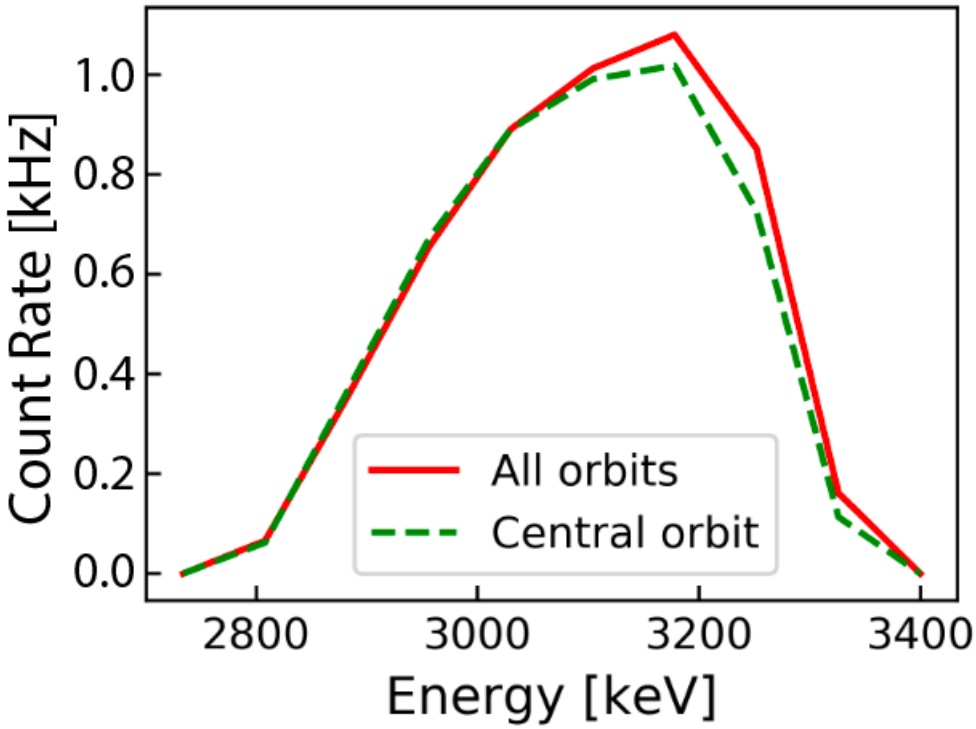

Figure 8: Comparison of the proton energy spectrum calculated using the true energy-dependent orbits and transmission factors (solid curve) with a calculation that employs identical orbits and transmission factors for all escaping proton energies (dashed).

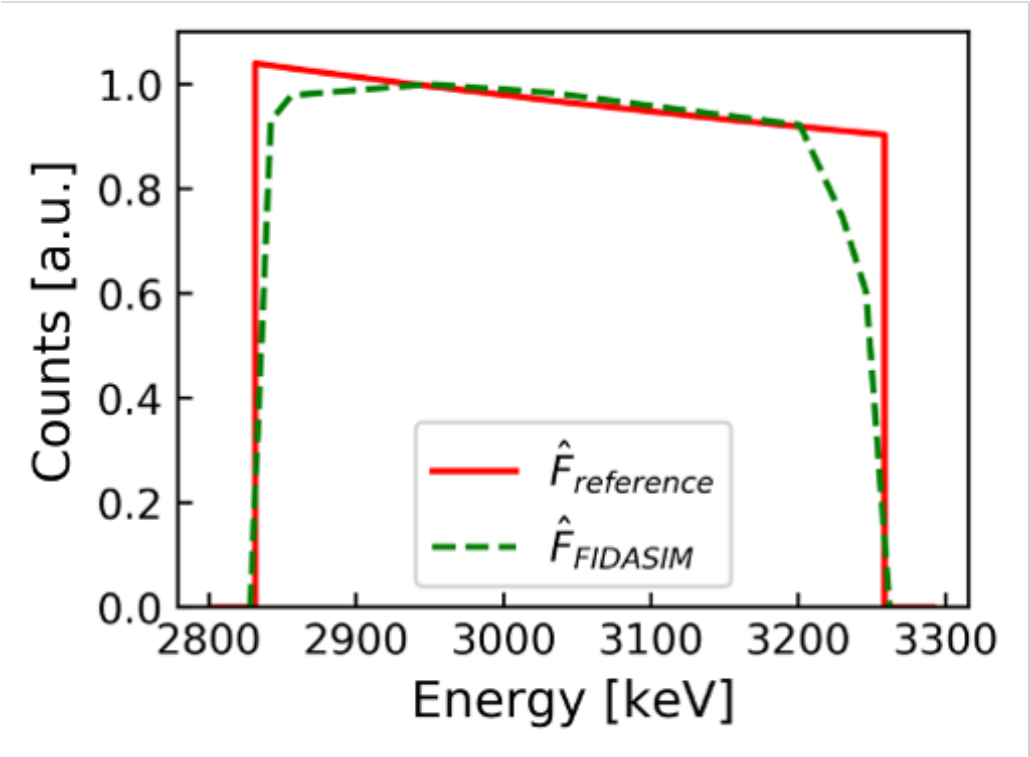

Figure 9: Proton energy spectrum for a monoenergetic (30 keV), isotropic, fast-ion distribution function in a plasma with nearly stationary deuterium target ions as computed by analytical theory (solid) and by FIDASIM (dashed).

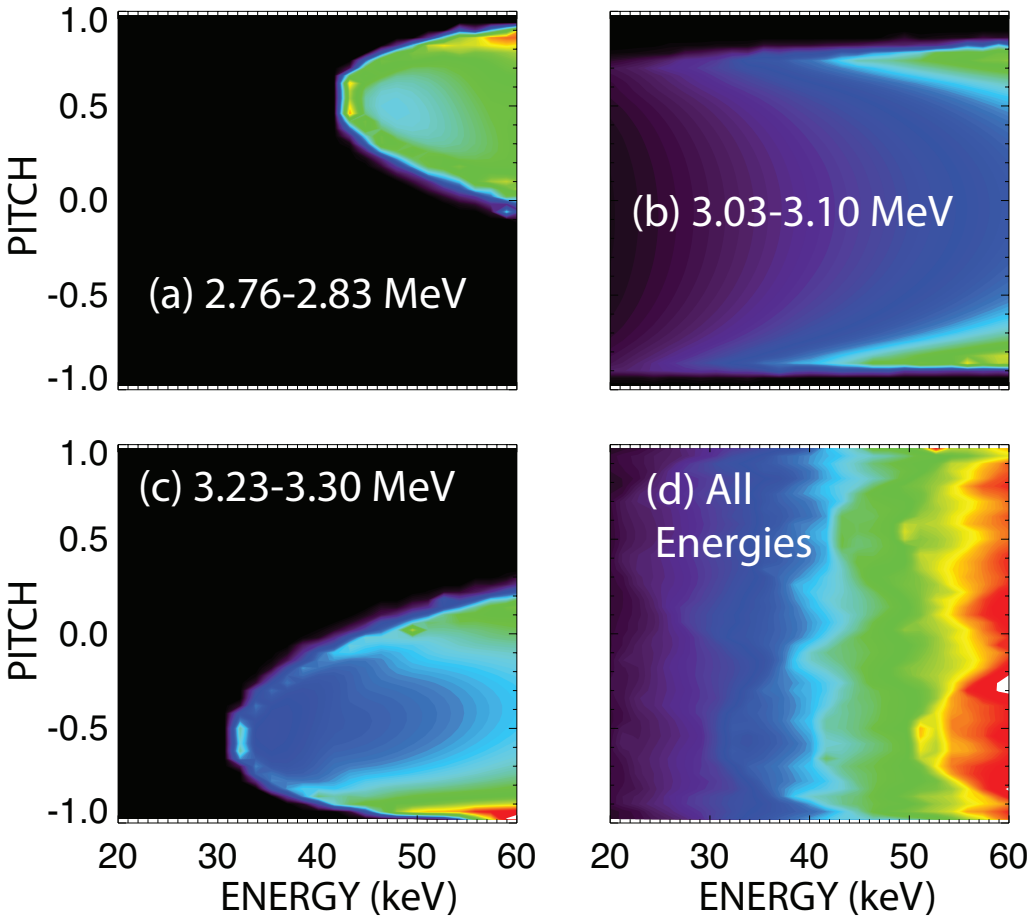

Figure 10: Velocity-space weight functions of a MAST 3-MeV proton channel for (a) down-shifted d-d protons, (b) unshifted protons, (c) up-shifted protons, and (d) protons of all energies. The abscissa is the fast-ion energy and the ordinate is $v_{\|}/v$ relative to the magnetic field. The same linear rainbow color table is employed in panels (a)-(c); in panel (d), the maximum value of the color table is 3.0 times larger.